EXPERIMENTAL STUDY ON DUCTILITY CAPACITY OF COMPOSITE BEAMS

S. Yamada[1], S.H. Oh[2], K. Okada[3]

1) Associate Professor, Structural Engineering Research Center, Tokyo Institute of Technology, Japan
naniwa@serc.titech.ac.jp
2) Research Institute of Industrial Science and Technology, Korea
oshoon@rist.re.kr
3) JSPS Research Fellow, Tokyo Institute of Technology, Japan
kokada@serc.titech.ac.jp

Abstract: Ductility capacity of composite beams which have conventional type of scallops has been investigated by cyclic loading tests. The results of the tests have shown that ductility capacity of composite beams is nearly half of that of steel beams without slabs. The effectiveness of application of improved connection details to a composite beam has been investigated. The improved connection details applied to the composite beams are No-weld-access-hole detail and RBS detail. They have improved ductility capacity of composite beams sufficiently.

1. INTRODUCTION

In Hyogo-ken Nanbu Earthquake, many fractures of bottom flanges occurred at beam-to-column connections of steel framed structures. After the earthquake, many researchers tried to resolve the issues about fractures and ductility capacity of steel members. However, most of them ignored effects of slabs even though composite beams, which consist of steel beams and RC slabs strongly connected each other by stud connectors, are generally used for actual buildings.

A schematic diagram of beam-to-column connections subjected to seismic force is shown in Fig. 1. In positive bending, because of the RC slab resisting compression, the full section of the beam is subjected to tensile force and the tensile strain in the bottom flange becomes excessive, so that the ductility capacity of the composite beams is considered to reduce. However, in current structural design, ductility capacity of composite beams is supposed to be equal to that of steel beams without slabs.

In this study, ductility capacity of composite beams is investigated experimentally, focusing on flange fractures which mainly determine ductility capacity of these beams.
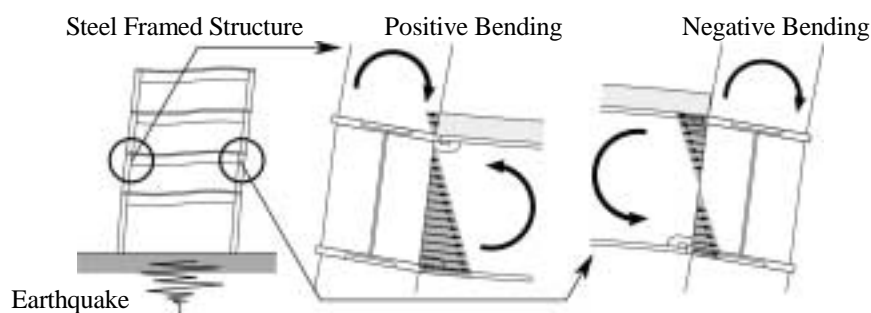
Fig. 1. Strain in Beam-to-column Connection under Earthquake

2. EXPERIMENTAL

A list of the specimens is shown in Table 1, and the standard specimen (No.1) is shown in Fig. 2. The scale and the shape of the specimens were designed based on those of beam-to-column connections of medium-rise steel buildings. The columns and the panels are composed of thick plates over 22mm so that they have sufficient strength to remain elastic during the tests. A list of mechanical properties of the materials used for the specimens is given in Table 2.

The specimens are divided into two series, Series A and Series B.

Series A (No.1~No.5) consists of four composite beam specimens (No.1, No.3~No.5) and one steel beam specimen without slabs (No.2). They have conventional type of weld access holes in their beam-to-column connections. The main purposes of the tests using Series A specimens are: (a) to demonstrate fractures of composite beams in Hyogo-ken Nanbu Earthquake; (b) to investigate ductility capacity of composite beams for fracture; and (c) to clarify the effects of slabs on ductility capacity of composite beams. Experimental parameters for Series A are as follows: (1) existence of a slab; (2) section properties; and (3) loading patterns.

Series B (No.6, No.7) consists of two composite beam specimens, beam-to-column connection details of which are modified to improve their ductility capacity. The details applied to Series B specimens are No-weld-access-hole detail (No.6) and RBS detail (No.7). No-weld-access-hole detail is shown in Fig. 3, and RBS detail is shown in Fig. 4. Many researchers have studied the effectiveness of these details in steel beams without slabs [Suita, et al]. The purpose of the tests using Series B specimens is to demonstrate their effectiveness in composite beams.

The experimental setup is shown in Fig. 5. During the tests, lateral deformation is restricted by frames positioned at the ends of the lateral beams and the free end of the main beam.

The deformation of the specimens is defined in Fig. 6 as the rotation angle θ. The actuator is controlled so that θ follows the target deformation shown in Fig. 7. Pattern 1 is applied to all specimens except No.5, and pattern 2 is applied to No.5 to investigate effects of the difference in the loading patterns.

Table 1. List of Specimens

	No.	Parameter	Beam	$_cM_p$ [kN·m]	$_sM_p$ [kN·m]	$_s\theta_p$ [rad.]	t_c [mm]	Weld Access Holes	Loading Pattern
	1	Standard	R-H-612×202×13×23	2.24×10³	1.41×10³	0.0082	200	Conventional	1
A	2	(1) Existence of a slab without Slab	R-H-612×202×13×23	---	1.41×10³	0.0082	0	Conventional	1
	3	(2) Section properties Small Section Beam	R-H-596×199×10×15	1.69×10³	0.99×10³	0.0087	200	Conventional	1
	4	(2) Section properties Thinner Slab	R-H-612×202×13×23	2.07×10³	1.41×10³	0.0082	140	Conventional	1
	5	(3) Loading pattern Pattern 2	R-H-612×202×13×23	2.24×10³	1.41×10³	0.0082	200	Conventional	2
B	6	(4) Improved connection details Non-Scallop detail	R-H-612×202×13×23	2.07×10³	1.33×10³	0.0077	200	Non-scallop	1
	7	(4) Improved connection details RBS detail	B-H-610×240×12×22 RBS: B-H-610×160×12×22	2.13×10³ 2.33×10³	1.43×10³ 1.12×10³	0.0077 ---	200	Conventional	1

$_cM_p$: full plastic moment calculation for composite beams [AIJ], $_sM_p$: full plastic moment calculation for bare steel beams, $_s\theta_p$: elastic rotation angle of bare steel beams subjected to $_sM_p$, t_c: thickness of slabs

Panel Thickness: 32mm
Beam: H-612x202x13x23
Loading Point

Column: Box-450x45x22

3000

3500
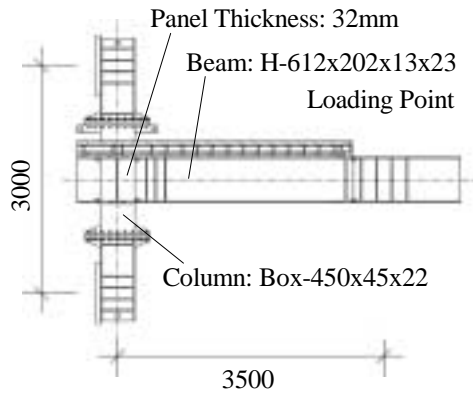
Fig. 2. Configuration of Specimen (No.1)

Table 2. Results of Material Tests

Material			σ_y [N/mm^2]	σ_υ [N/mm^2]	Y.R. [%]	ε_υ [%]
SM490	H-612x202x13x23 (No.1,2,4,5)	Flange	386	535	72.2	14.4
		Web	444	551	80.6	14.6
	H-612x202x13x23 (No.6)	Flange	351	522	67.3	17.6
		Web	353	539	65.5	17.4
	H-596x199x10x15 (No.3)	Flange	414	556	74.5	14.4
		Web	445	565	78.8	14.4
	PL-22(No.7)	Flange	376	501	75.0	13.9
	PL-12(No.7)	Web	357	565	63.2	14.4
Concrete (Fc=23.5N/mm^2)		28days	---	26.0	---	---

σ_y: yield stress, σ_u: maximum stress, Y.R.: yield ratio, ε_u: elongation

Conventional
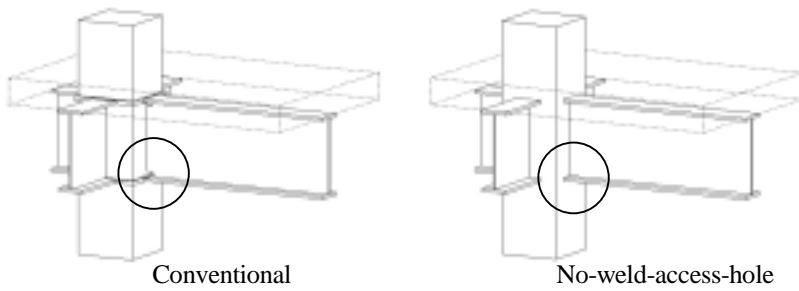
No-weld-access-hole

Fig. 3. No-weld-access-hole Detail

Fig. 4. RBS Detail

Actuator (2000kN)

Reaction Wall

Specimen

Pin Joint

Fig. 5. Testing Setup

θ

Fig. 6. Rotation Angle θ

$+8_s\theta_p$
$+6_s\theta_p$
$+4_s\theta_p$
$+2_s\theta_p$
$-2_s\theta_p$
$-4_s\theta_p$
$-6_s\theta_p$
$-8_s\theta_p$

Pattern 1

$+5_s\theta_p$
$+4_s\theta_p$
$+3_s\theta_p$
$+2_s\theta_p$
$-2_s\theta_p$
$-3_s\theta_p$
$-4_s\theta_p$
$-5_s\theta_p$
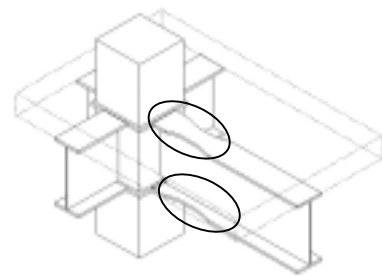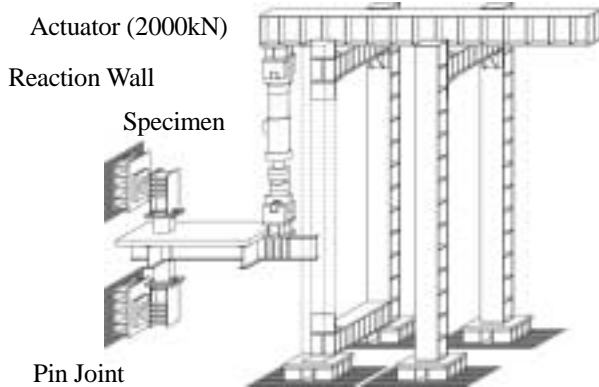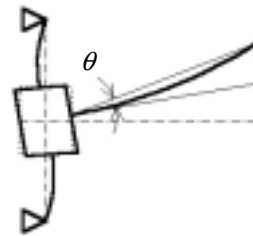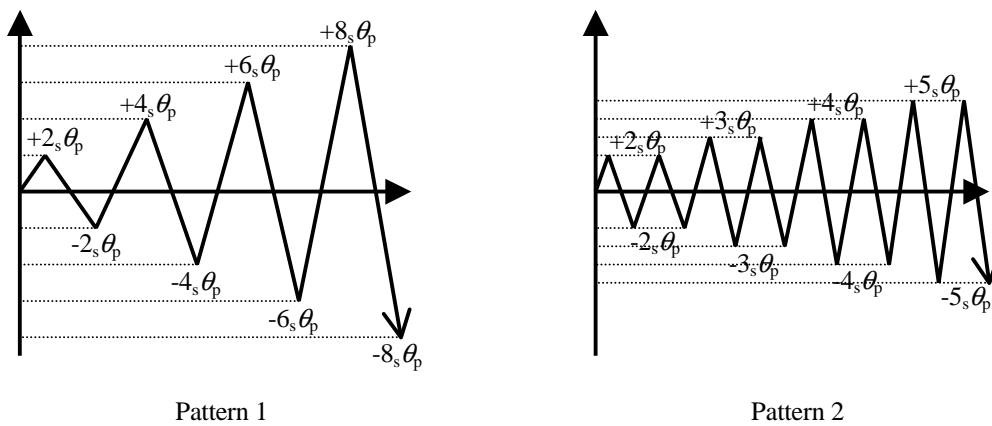
Pattern 2

Fig. 7. Loading Patterns

3. RESULTS & DISCUSSION

3.1. Experimental results & Ductility capacity

Moment (M) versus rotation angle (θ) relationships are shown in Fig. 8, where   shows the point where the flange fracture occurred. Full plastic moment calculations for composite beams and steel beams are shown by dashed lines as $_cM_p$ and $_sM_p$. Some experimental results are listed in Table 3.

The failure mode of all the specimens in Series A is flange fracture initiated by a crack which occurred at the tip of a weld access hole. The flange fractures of the composite beam specimens occurred in positive bending state.

The ductility capacity of specimens in Series A is compared by θ^+_{max} and $_s\theta^+_{max}$, where θ^+_{max} is the maximum rotation angle in positive bending state in M-θ relationships, and $_s\theta^+_{max}$ is the maximum rotation angle in positive bending state in skeleton curves. The skeleton curves are converted from M-θ relationships in the way shown in Fig. 9, and they are shown in Fig. 10. θ^+_{max} and $_s\theta^+_{max}$ of specimens in Series A are compared in Fig. 11. θ^+_{max} of the composite beams are 50~60% and $_s\theta^+_{max}$ of them are 40~50% when comparing to steel beam without slabs (No.2). Differences in section properties and loading patterns have little effect on their deformation capacity.

The specimens in Series B (No.6, No.7) were tested until flange fractures occurred. The deformation capacity of them is higher than that of the composite beams in Series A, and even that of the steel beam specimen without slab (No.2).

No.1: Standard Composite Beam

No.2: Bare Steel Beam

No.3: Small Section Beam

No.4: Thinner Slab

No.5: Loading Pattern 2

No.6: No-weld-access-hole Detail

No.7: RBS Detail
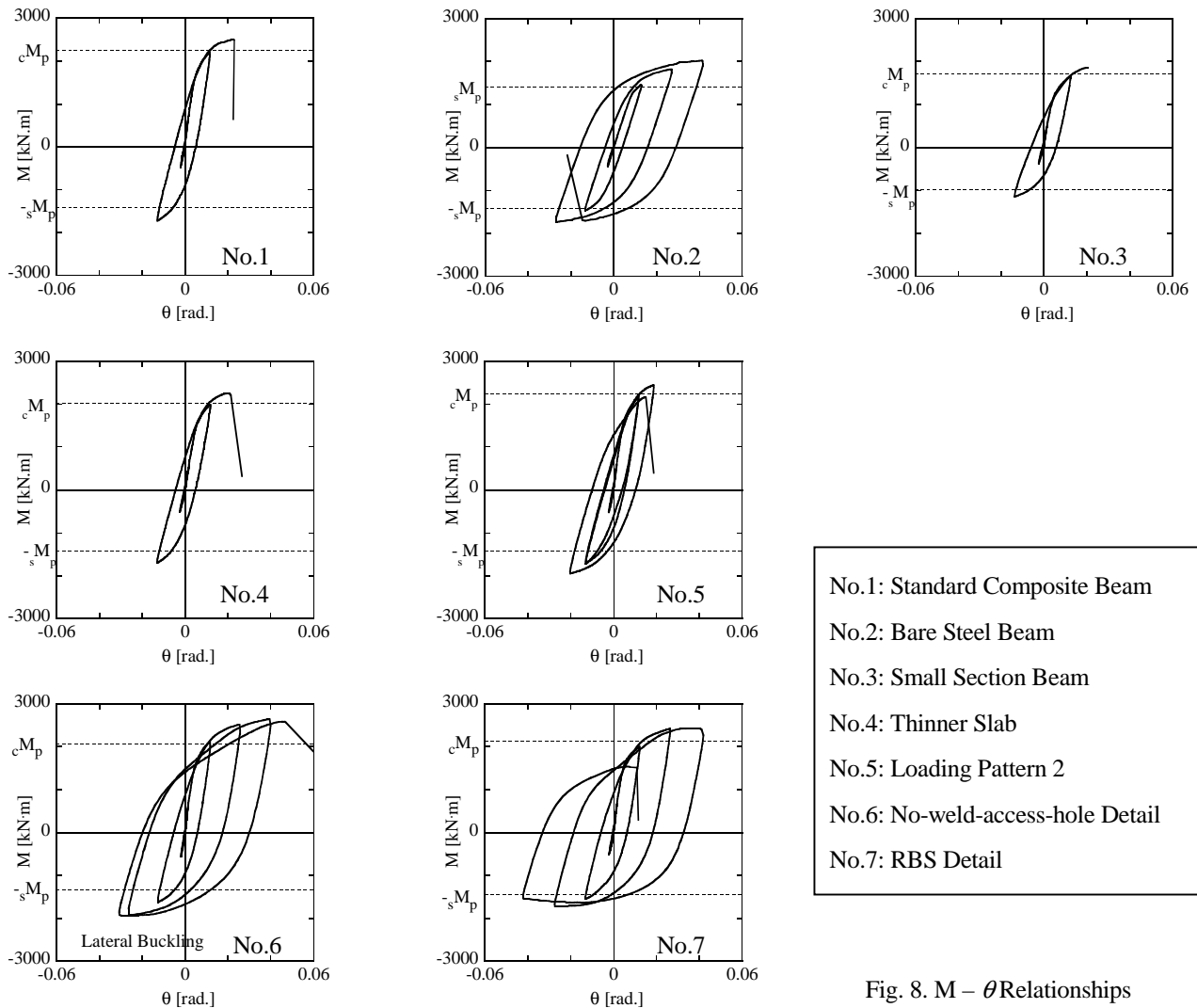
Fig. 8. M – θ Relationships

Table 3. Results of Tests

No.	K_e^+ [kN·m/rad.]	K_e^- [kN·m/rad.]	M_{max}^+ [kN·m]	M_{max}^- [kN·m]	θ_{max}^+ [rad.]	θ_{max}^- [rad.]	Fracture Part	Failure Mode	Temp. [°C]
1	412000	262000	2500	-1730	0.0231	-0.0129	Bottom Flange	Brittle Fracture	29.0
2	157000	----	2020	-1710	0.0416	-0.0268	Top Flange	Brittle Fracture	29.0
3	307000	185000	1860	-1150	0.0206	-0.0138	Bottom Flange	Ductile Fracture	29.0
4	314000	233000	2250	-1710	0.0214	-0.0131	Bottom Flange	Brittle Fracture	28.5
5	377000	262000	2440	-1950	0.0187	-0.0203	Bottom Flange	Brittle Fracture	28.5
6	477000	312000	2650	-1930	0.0470	-0.0308	Bottom Flange	Ductile Fracture	19.5
7	423000	279000	2430	-1720	0.0419	-0.0423	Bottom Flange	Brittle Fracture	28.5

K_e^+: initial stiffness under positive bending, K_e^-: initial stiffness under negative bending, M_{max}^+: maximum moment under positive bending, M_{max}^-: maximum moment under negative bending, θ_{max}^+: maximum rotation angle under positive bending, θ_{max}^-: maximum rotation angle under negative bending, Temp.: temperature
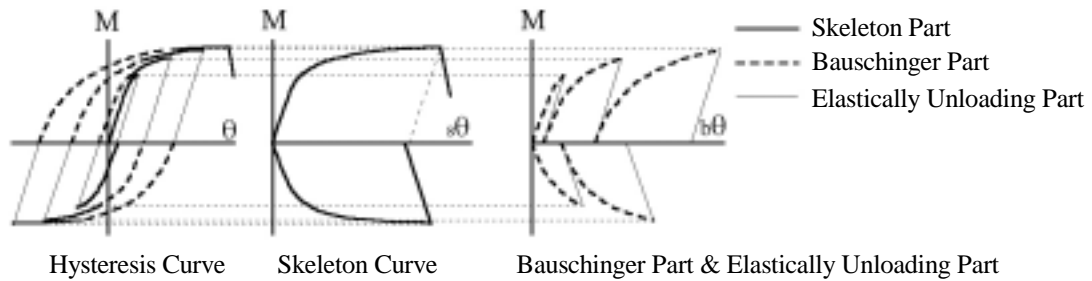
Fig. 9. Concept of Skeleton Curves
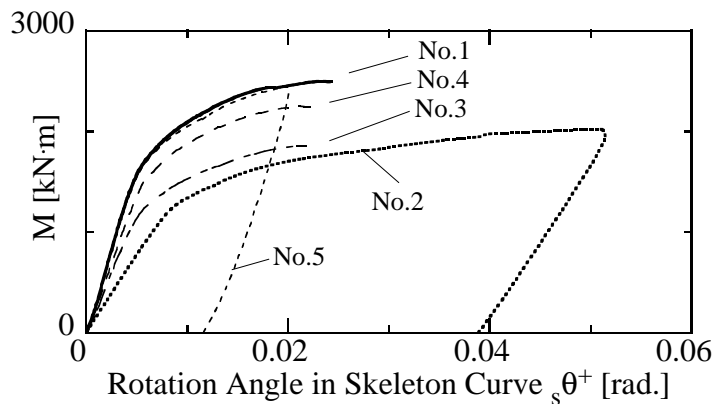
Fig. 10. Skeleton Curves (Series A)
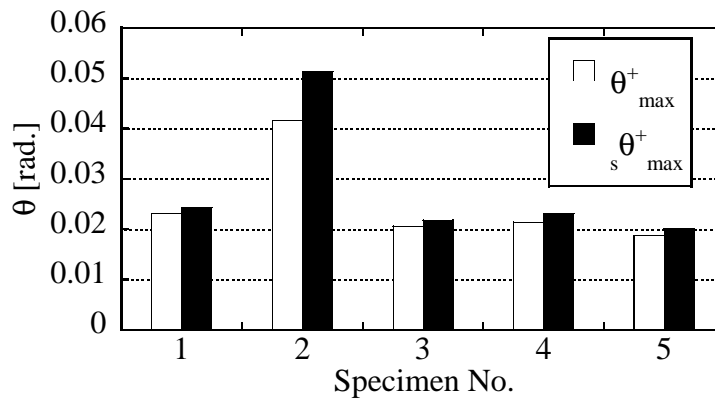
Fig. 11. Ductility Capacity (Series A)

3.2. Effects of a slab on ductility capacity of composite beams

Focusing on the existence of slabs, the effect of the slab on ductility capacity is investigated from the result of No.1 and No.2. The strain data are measured in two sections, Section A and Section B, shown in Fig. 12. The examples of strain distributions for Section A under positive bending are also shown in Fig. 12. The strain in the bottom flange of No.1 is larger than that of No.2, so that the neutral axis of No.1 seems to have moved to the upper flange side. This is the main reason for reduction of ductility capacity of composite beams.

Moment (M) versus curvature (ϕ) relationships can be obtained from the strain data in each section. The positive bending part of the skeleton curves of M-ϕ relationships are shown in Fig. 13. The ductility capacity around Section A (near the fracture point) is compared by the maximum curvature. The ductility capacity around Section A of No.1 is 65% of that of No.2.

As shown in Fig. 13, a restoring force of Section A is higher than that of Section B at same curvature. The difference in restoring forces between Section A and Section B of No.1 is about 35%, and that of No.2 is about 20%. This indicates that Section A of No.1 is relatively weaker than that of No.2, and that the deformation around the beam-to-column connection tends to be larger in No.1 than No.2, so that No.1 has reduced the ductility capacity. The curvature distribution diagrams for No.1 and No.2 specimens are shown in Fig. 14, and these are obtained at the maximum rotation angle of Fig. 10. It is shown that the plastic zone of No.1 was narrow and concentrated to the beam-to-column connection when flange fracture occurred.
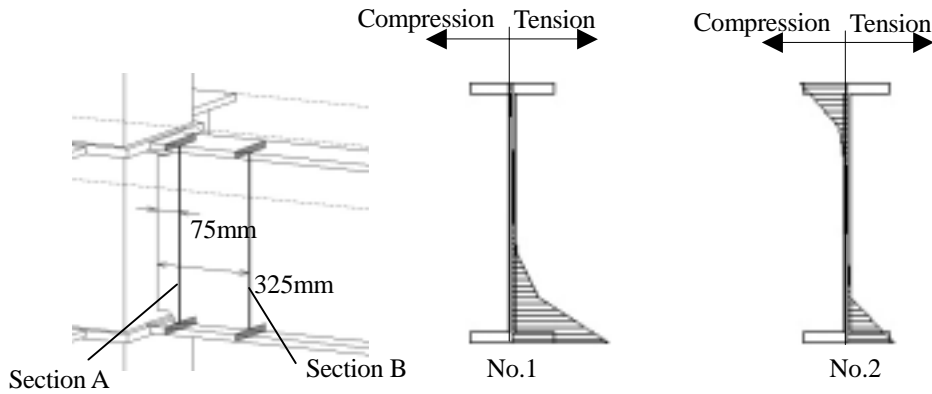
Fig. 12. Strain Distribution Diagrams
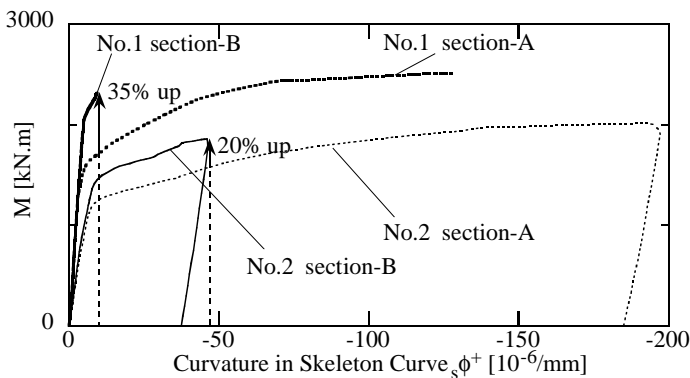
Fig. 13. Skeleton Curves of Moment versus Curvature Relationships

(No.1, No.2)
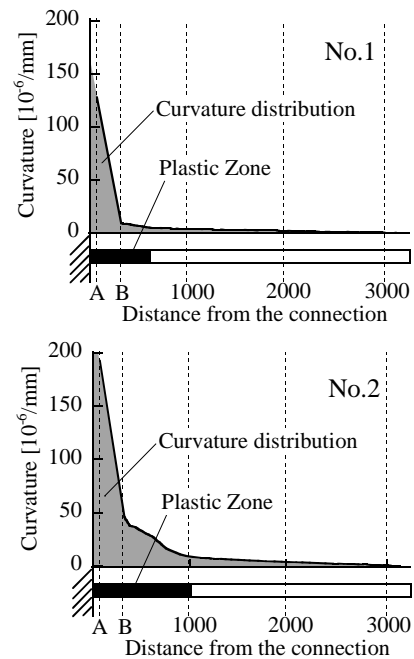
Fig. 14. Curvature Distribution

3.3. Effectiveness of improved connection details in composite beams

Skeleton curves of M-ϕ relationships for No.6 and No.7 specimens are shown in Fig. 15. For No.6, a restoring force of Section A is 25% larger than that of Section B, and for No.7, a restoring force of Section A is equal to that of the smallest section in RBS area. This data implies that if beam-to-column connections are protected from concentration of deformation, the deformation capacity of composite beams is improved.
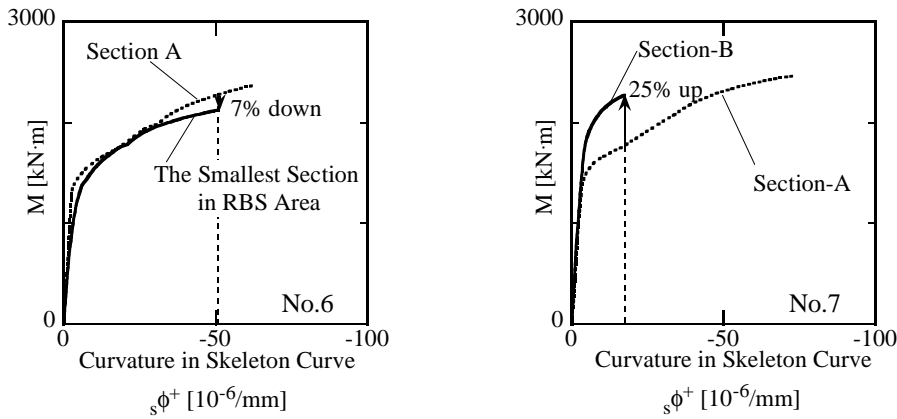
Fig. 15. Skeleton Curves of Moment versus Curvature Relationships (No.6, No.7)

4. CONCLUSION

In this study, ductility capacity of composite beams is investigated by cyclic loading tests. The results indicate that ductility capacity of composite beam is nearly half of that of steel beams without slabs. This is due to slabs, the effects of which are considered as the strain concentration to the bottom flange and the deformation concentration to the beam-to-column connection. And, No-weld-access-hole detail and RBS detail improve ductility capacity of composite beams sufficiently.

References:
A.I.J. (1998) Recommendation for Limit State Design of Steel Structures, Architectural Institute of Japan.
Suita, K. et al (1999), "Plastic rotation capacity of steel beam-to-column connections using a reduced beam section and no weld access hole design -Full scale tests for improved steel beam-to-column subassemblies -part 1-", *J. Struct. & Const. Eng.*, A.I.J., No. 526, 177-184.